

# Studies of the Structure and Properties of Amorphous $a\text{-Zr}_{76}\text{Fe}_{24}\text{H}_x$

R. C. BOWMAN, JR.  
Chemistry and Physics Laboratory  
The Aerospace Corporation  
El Segundo, CA 90245

A. J. MAELAND  
Allied/Signal Corporation  
Morristown, NJ 07960

K. M. UNRUH  
Department of Physics  
University of Delaware  
Newark, DE 19716

E. L. VENTURINI  
Sandia National Laboratories  
Albuquerque, NM 87185

J. J. RUSH  
National Bureau of Standards  
Gaithersburg, MD 20899

J. S. CANTRELL  
Chemistry Department  
Miami University  
Oxford, OH 45056

31 May 1989

Prepared for

AIR FORCE SPACE TECHNOLOGY CENTER  
Kirtland Air Force Base, NM 87117

SPACE SYSTEMS DIVISION  
AIR FORCE SYSTEMS COMMAND  
Los Angeles Air Force Base  
P.O. Box 92960  
Los Angeles, CA 90009-2960

APPROVED FOR PUBLIC RELEASE;  
DISTRIBUTION UNLIMITED

DTIC  
ELECTE  
NOV 06 1989  
S E D

AD-A214 646

## REPORT DOCUMENTATION PAGE

1a. REPORT SECURITY CLASSIFICATION Unclassified		1b. RESTRICTIVE MARKINGS	
2a. SECURITY CLASSIFICATION AUTHORITY		3. DISTRIBUTION/AVAILABILITY OF REPORT Approved for public release; distribution unlimited	
2b. DECLASSIFICATION/DOWNGRADING SCHEDULE			
4. PERFORMING ORGANIZATION REPORT NUMBER(S) TR-0088(3057)-2		5. MONITORING ORGANIZATION REPORT NUMBER(S) SD-TR-89-70	
6a. NAME OF PERFORMING ORGANIZATION The Aerospace Corporation Laboratory Operations	6b. OFFICE SYMBOL (If applicable)	7a. NAME OF MONITORING ORGANIZATION Space Systems Division	
6c. ADDRESS (City, State, and ZIP Code) El Segundo, CA 90245		7b. ADDRESS (City, State, and ZIP Code) Los Angeles Air Force Base Los Angeles, CA 90009-2960	
8a. NAME OF FUNDING/SPONSORING ORGANIZATION Air Force Space Technology Center	8b. OFFICE SYMBOL (If applicable)	9. PROCUREMENT INSTRUMENT IDENTIFICATION NUMBER F04701-85-C-0086-P00019	
8c. ADDRESS (City, State, and ZIP Code) Kirtland Air Force Base, NM 87117		10. SOURCE OF FUNDING NUMBERS	
		PROGRAM ELEMENT NO.	PROJECT NO.
		TASK NO.	WORK UNIT ACCESSION NO.
11. TITLE (Include Security Classification) Studies of the Structure and Properties of Amorphous $a\text{-Zr}_{76}\text{Fe}_{24}\text{H}_x$			
12. PERSONAL AUTHOR(S) Bowman, R. C., Jr., Maeland, A. J. (Allied/Signal); Unruh, K. M. (U. Delaware); Venturini, E. L. (Sandia); Rush, J. J. (National Bureau of Standards); Cantrell, J. S. (Miami U.)			
13a. TYPE OF REPORT	13b. TIME COVERED FROM _____ TO _____	14. DATE OF REPORT (Year, Month, Day) 1989 May 31	15. PAGE COUNT 9
16. SUPPLEMENTARY NOTATION			
17. COSATI CODES		18. SUBJECT TERMS (Continue on reverse if necessary and identify by block number)	
FIELD	GROUP	SUB-GROUP	
		amorphous alloys, hydrogen in metals, thermal stability of amorphous alloys, electronic structure in metal hydrides, Mössbauer effect application, nuclear magnetic resonance.	
19. ABSTRACT (Continue on reverse if necessary and identify by block number) The $a\text{-Zr}_{76}\text{Fe}_{24}\text{H}_x$ samples with $x \leq 173$ have been shown to remain amorphous after reaction of the glassy alloy with gaseous hydrogen. Magnetic susceptibility and Mössbauer spectroscopy indicate that the electronic structure of the alloy is modified upon hydrogen absorption. Proton spin-lattice relaxation times suggest a strong hyperfine interaction with the iron d-states. The vibrational spectrum of $a\text{-Zr}_{76}\text{Fe}_{24}\text{H}_{173}$ from inelastic neutron scattering shows hydrogen occupancy in a distribution of tetrahedral interstitial sites. Calorimetry and x-ray diffraction demonstrate that $a\text{-Zr}_{76}\text{Fe}_{24}\text{H}_x$ with $x > 140$ irreversibly crystallizes into $c\text{-ZrH}_x$ and $\text{ZrFe}_2$ .			
20. DISTRIBUTION/AVAILABILITY OF ABSTRACT <input checked="" type="checkbox"/> UNCLASSIFIED/UNLIMITED <input type="checkbox"/> SAME AS RPT. <input type="checkbox"/> DTIC USERS		21. ABSTRACT SECURITY CLASSIFICATION Unclassified	
22a. NAME OF RESPONSIBLE INDIVIDUAL		22b. TELEPHONE (Include Area Code)	22c. OFFICE SYMBOL

PREFACE

We wish to thank Dr. S. H. Liou, J. E. Wagner, and T. Beiter for help with the measurements. The work at the Sandia National Laboratories was supported by the U. S. Department of Energy under Contract No. DE-AC04-76-DP00789. The work at The Aerospace Corporation was supported by the U. S. Air Force Space Division under Contract No. F04701-85-C-0086-P00019.

Accession For	
NTIS GRA&I	<input checked="" type="checkbox"/>
DTIC TAB	<input checked="" type="checkbox"/>
Unannounced	<input type="checkbox"/>
Justification	
By _____	
Distribution/	
Availability Codes	
Dist	Avail and/or Special
A-1	

During the past decade, the formation of amorphous hydrides from glassy or crystalline alloys has been widely studied.<sup>1</sup> Since the Zr-based metallic glasses can often absorb large quantities of hydrogen without crystallization, the properties of these amorphous hydrides are especially interesting.<sup>2-5</sup> Fries, et al.<sup>6, 7</sup> have studied several glassy  $a\text{-Zr}_{1-y}\text{Fe}_y$  alloys before and after electrolytic charging with hydrogen. They reported an unusually large hydrogen absorption for the  $y = 0.24$  glass—namely, the nominal maximum composition  $a\text{-Zr}_{76}\text{Fe}_{24}\text{H}_{246}$ . The present work describes evaluations of  $a\text{-Zr}_{76}\text{Fe}_{24}\text{H}_x$  samples prepared by reacting the glassy alloy with hydrogen gas.

The  $a\text{-Zr}_{76}\text{Fe}_{24}$  glass was produced by conventional melt-spinning. X-ray diffraction (XRD) did not show any crystalline components in these ribbons, and the alloy density was found to be  $6.81(2) \text{ g/cm}^3$ . The alloy was reacted at room temperature with hydrogen gas where the initial pressures were slightly above one atmosphere. Thermal desorption measurements<sup>4,5</sup> on the powdered product gave a saturated composition of  $a\text{-Zr}_{76}\text{Fe}_{24}\text{H}_{173}$ . Figure 1 presents the XRD pattern from some of this hydrided material. There is no evidence of any crystalline phases, and the decrease in the peak position (i.e., at  $2\Theta_p = 33.7^\circ$ ) relative to the value for the initial glass (i.e.,  $2\Theta_p = 36.3^\circ$ ) corresponds to a net volume expansion of  $2.67\text{\AA}^3/\text{H-atom}$ .

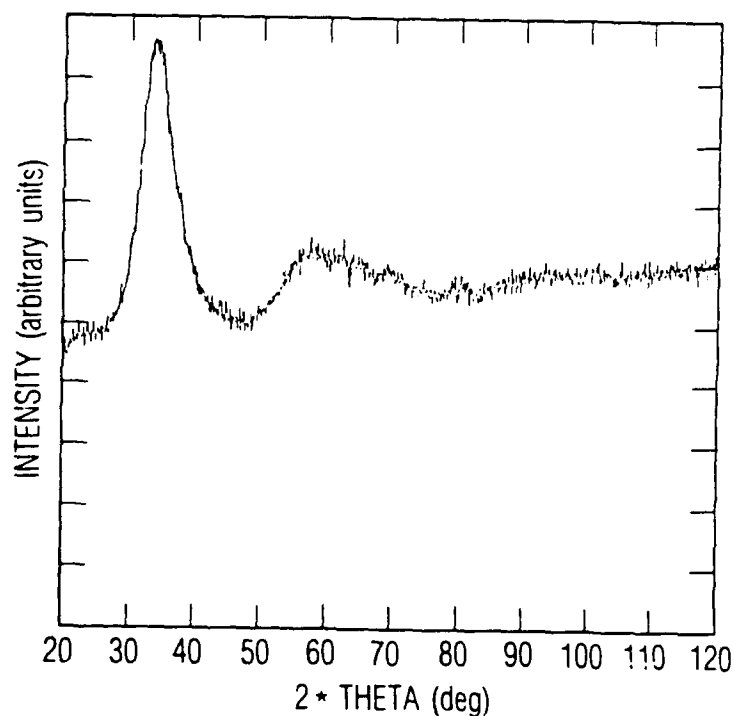


Fig 1. X-ray Diffraction Pattern for  $a\text{-Zr}_{76}\text{Fe}_{24}\text{H}_{173}$  Obtained with  $\text{Cu K}\alpha$  Radiation.

In order to obtain insight into the hydrogen site occupancy, an inelastic neutron scattering (INS) study was made on  $a\text{-Zr}_{76}\text{Fe}_{24}\text{H}_{173}$ ; its room temperature vibrational spectrum is shown in Figure 2. The peak maximum is at 137(4) MeV, and the full-width half maximum is 63(6) MeV. These values are very close to the INS results for other amorphous Zr-based hydrides where hydrogen atoms predominantly occupy tetrahedral sites with mostly Zr neighbors.<sup>5</sup> However, the large linewidths imply considerable distortions and possibly some occupancy of sites with different symmetries.<sup>5</sup>

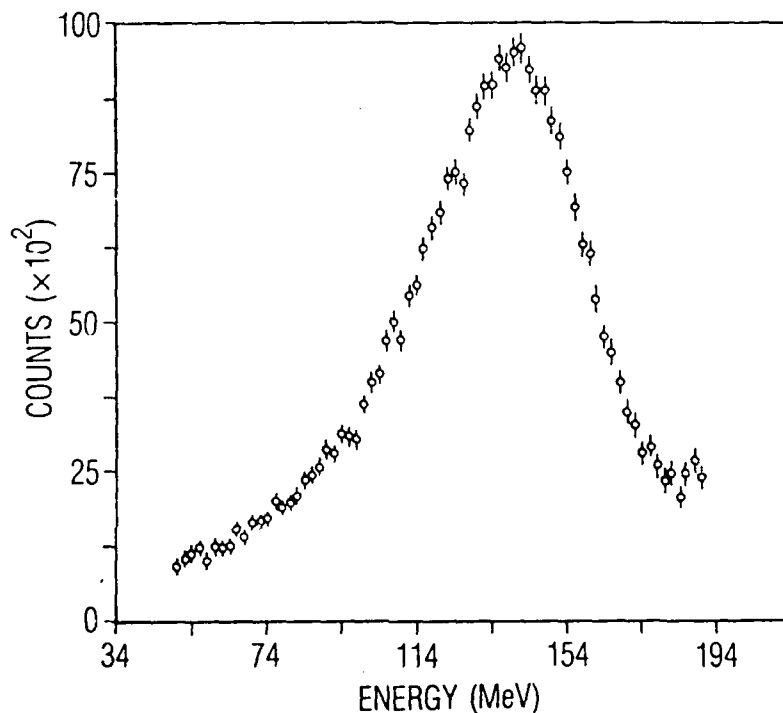


Fig 2. Hydrogen Vibration Spectrum for  $a\text{-Zr}_{76}\text{Fe}_{24}\text{H}_{173}$  from Inelastic Neutron Scattering Measurement at Room Temperature.

A previously described<sup>2</sup> SQUID magnetometer was used to determine magnetic properties between 7 K and 300 K for magnetic fields up to 40kOe. The magnetic susceptibilities  $\chi(T)$  for three  $a\text{-Zr}_{76}\text{Fe}_{24}\text{H}_x$  samples are shown in Figure 3. The glassy alloy  $a\text{-Zr}_{76}\text{Fe}_{24}$  exhibits Pauli paramagnetism with  $\chi(T)$  being nearly temperature-independent, which contrasts with some past measurements.<sup>8,9</sup> However,  $\chi(T)$  curves for the amorphous hydrides show a Curie-Weiss term, which is most likely due to superparamagnetic Fe clusters or iron oxides produced by surface decomposition during hydriding. As shown in Table I, the Pauli terms  $\chi(0)$  for the hydrides are equal or even 10% smaller than for the alloy.

Nuclear magnetic resonance (NMR) determinations of the proton spin-lattice relaxation times ( $T_1$ ) have provided useful assessments of the electronic structures of many

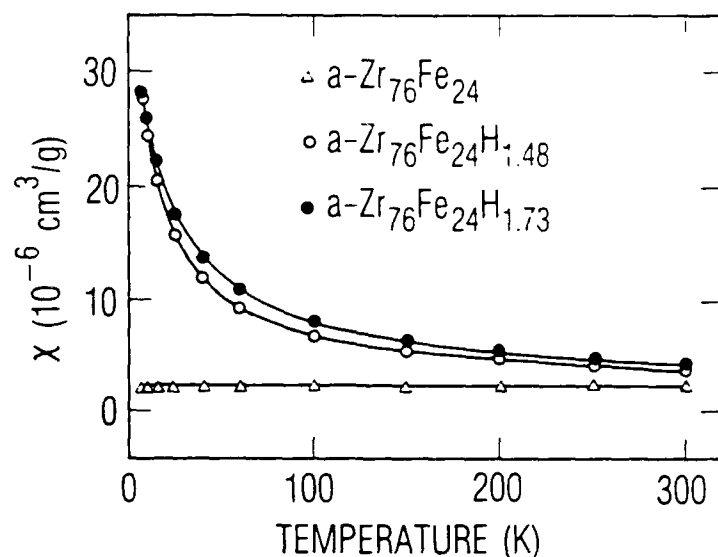


Fig. 3. Temperature Dependence of Magnetic Susceptibilities ( $\chi$ ) Where the Curves Are Least-square Fits with  $\chi(T) = \chi(0)\{1 + BT\}$  for the Alloy and  $\chi(T) = \chi(0) + C/T + \Theta$  for the Amorphous Hydrides.

Table I. Summary of Various Parameters from  $a\text{-Zr}_{76}\text{Fe}_{24}\text{H}_x$  Samples. See text for definitions.

x	$\chi(0)$ ( $10^{-6}\text{cm}^3/\text{g}$ )	$\overline{IS}$ (mm/s)	$\overline{QS}$ (mm/s)	$(T_1T)^{-1/2}$ ( $\text{s} \cdot \text{K}$ ) $^{-1/2}$	$T_{\text{exo}}$ (K)	$T_{\text{endo}}$ (K)
0	2.27	-0.263	0.55	—	663,802	—
148	2.33	+0.270	0.49	0.64	541	552
173	1.99	+0.272	0.49	0.61	534	542

crystalline and amorphous hydrides.<sup>3, 5, 10, 11</sup> Figure 4 summarizes the proton  $T_1$  results obtained at 34.5 MHz on the two  $a\text{-Zr}_{76}\text{Fe}_{24}\text{H}_x$  samples. Table I contains the  $(T_1T)^{-1/2}$  parameters [which are directly proportional to the density ( $N_F$ ) of electronic states at the Fermi level].<sup>3, 10</sup> When compared with values for other amorphous Zr-based hydrides,<sup>3, 5, 10</sup> the  $(T_1T)^{-1/2}$  data in Table I are nearly an order of magnitude larger. However, this differ-

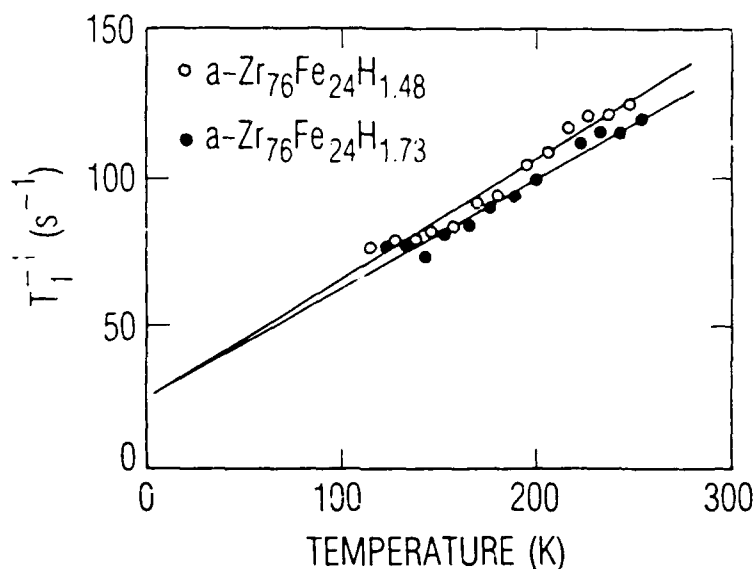


Fig. 4. Inverse Proton Spin-Lattice Relaxation Times Where the Korringa Parameters ( $T_1T$ ) Are Derived from the Slopes of the Solid Lines.

ence is not believed to reflect an unusually large  $N_F$  but rather a very strong hyperfine interaction with the Fermi level iron d-states as was previously found in crystalline  $\text{TiFeH}_x$ .<sup>11</sup> Presumably, the electronic structure of  $a\text{-Zr}_{76}\text{Fe}_{24}\text{H}_x$  has the iron states sufficiently near the Fermi level to influence the protons via a polarization mechanism.<sup>10</sup>

The Mössbauer spectra of the  $^{57}\text{Fe}$  isotope were obtained at room temperature and at 4.2 K in conventional transmission geometry. Two 4.2 K spectra are shown in Figure 5, along with fits using the distributions of quadrupole splittings  $P$  (QS) obtained by a modification of Window's method.<sup>12</sup> Both  $a\text{-Zr}_{76}\text{Fe}_{24}$  alloy and  $a\text{-Zr}_{76}\text{Fe}_{24}\text{H}_{1.73}$  are paramagnetic at this temperature (as well as room temperature—see Fries, et al.<sup>6, 7</sup>). Furthermore, there is no indication of ferromagnetic iron precipitates in these Mössbauer spectra. However, the suspected magnetic Fe clusters<sup>13</sup> require the conversion electron Mössbauer technique for this direct detection. The mean isomer shifts ( $\bar{IS}$ ) referred to  $\alpha\text{-Fe}$  and quadrupole splittings ( $\bar{QS}$ ) obtained at RT are presented in Table I. As reported by Fried, et al.<sup>6, 7</sup> hydrogenation of  $a\text{-Zr}_{76}\text{Fe}_{24}$  causes a substantial increase in  $\bar{IS}$  that probably reflects changes in electronic structure<sup>14</sup> (e.g., a partial charge transfer from Fe to H) in addition to a contribution from the volume expansion. The quadrupole splitting distributions in Figure 5 indicate a significant increase in the near-zero range for the hydride, suggesting some structural changes to give iron symmetries that are more nearly cubic<sup>6</sup> than in the original glassy alloy.

The thermal stabilities of  $a\text{-Zr}_{76}\text{Fe}_{24}\text{H}_x$  have been studied by differential scanning calorimetry (DSC) and XRD after quenching from different temperatures.<sup>4, 5</sup> Representative

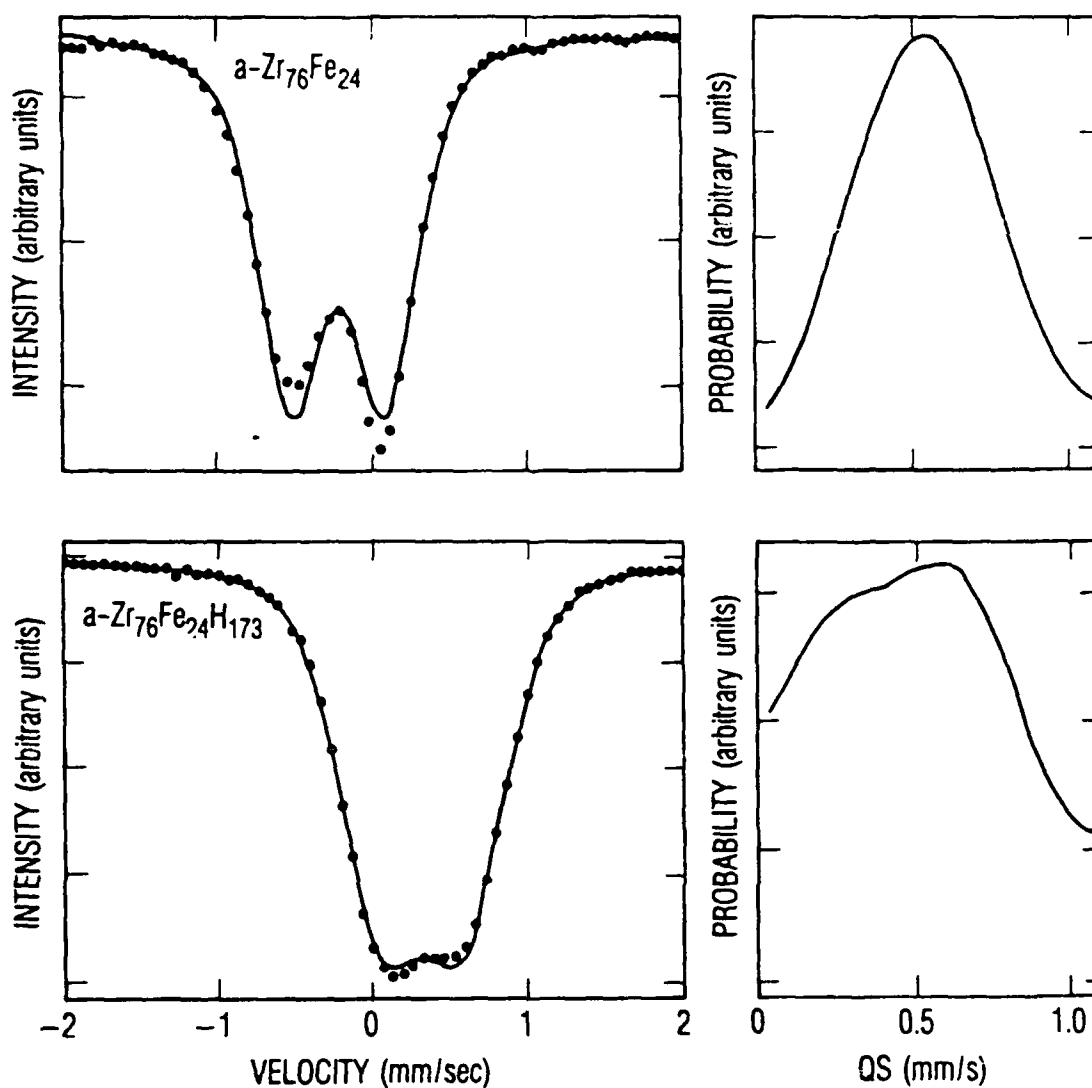


Fig 5. Mössbauer Spectra for Two  $a\text{-Zr}_{76}\text{Fe}_{24}\text{H}_x$  Samples Obtained at 4.2 K. The solid curves are fits through the data with the distributions of quadrupole splittings  $P(QS)$  shown on the right side.

DSC curves are presented in Figure 6, where the exothermic peaks ( $T_{\text{exo}}$ ) indicate crystallization or phase transitions<sup>4,5</sup> and the endothermic peak ( $T_{\text{endo}}$ ) corresponds to hydrogen evolution.<sup>4,5</sup> The peak temperatures are summarized in Table I. From the XRD results, the alloy  $a\text{-Zr}_{76}\text{Fe}_{24}$  initially crystallizes at 663 K to form hexagonal  $\omega\text{-Zr}$  and cubic  $\text{Zr}_2\text{Fe}$  but subsequently transforms into orthorhombic  $\text{Zr}_3\text{Fe}$  above 802 K. Additional information on  $a\text{-Zr}_{1-y}\text{Fe}_y$  crystallization is given by Cantrell and Bowman<sup>4</sup> and Matsuura.<sup>15</sup> The DSC measurements show that  $a\text{-Zr}_{76}\text{Fe}_{24}\text{H}_x$  crystallizes at a much lower temperature than the alloy. Furthermore, XRD indicated that  $\text{ZrH}_x$  formed during crystallization with a complementary intermetallic phase  $\text{ZrFe}_2$  for the highest quench temperature. Our results differ

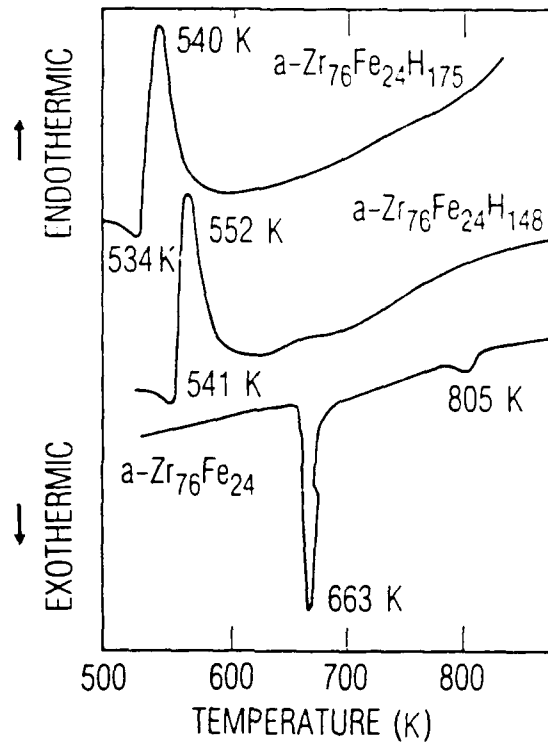


Fig. 6. DSC Traces for Heating Rates of 20 K/min.

from those for electrolytically charged  $a\text{-Zr}_{76}\text{Fe}_{24}\text{H}_{220}$ ,<sup>6</sup> where no  $\text{ZrH}_x$  or  $\text{ZrFe}_2$  was detected but the ternary oxide  $\text{Zr}_2\text{FeO}_x$  was found instead. Electrolytic charging probably introduced sufficient oxygen impurities to alter the phases formed during crystallization and inhibited the endothermic loss of hydrogen seen in Figure 6 from the  $a\text{-Zr}_{76}\text{Fe}_{24}\text{H}_x$  samples produced with hydrogen gas. It is noteworthy that these latter samples yielded  $\text{ZrH}_x$  as the major decomposition product, which was found when several other Zr-based amorphous hydrides<sup>4, 5</sup> underwent crystallization.

## REFERENCES

1. G. Bambakidis and R. C. Bowman, Jr. (editors), Hydrogen in Disordered and Amorphous Solids, Plenum, New York [1986].
2. E. L. Venturini, R. C. Bowman, Jr. and J. S. Cantrell, J. Appl. Phys. 57, 3542 [1985].
3. R. C. Bowman, Jr., in Reference 1, p. 237.
4. J. S. Cantrell and R. C. Bowman, Jr., Mat. Res. Soc. Symp. Proc. 80, 105 [1987].
5. R. C. Bowman, Jr., et al., Phys. Rev. B 37, 8575 [1988].
6. S. M. Fries, et al., J. Phys. F: Met. Phys 15, 1179 [1985].
7. S. M. Fries, et al., J. Magn. Mat. 54-57, 287 [1986].
8. L. Hedman and O. Rapp, Phys. Lett. A 100, 251 [1984].
9. S. N. Kaul, Phys. Lett. A. 100, 254 [1984].
10. R. C. Bowman, Jr., Hyperfine Inter. 24-26, 583 [1985].
11. J. S. Cantrell and R. C. Bowman, Jr., J. Less-Common Met. 130, 69 [1987].
12. B. Window, J. Phys. E: Sci. Instr. 4 [1971].
13. A. Bläslius and U. Gonser, Appl. Phys. 22, 331 [1980].
14. M. Gupta, Solid State Commun. 42, 501 [1982].
15. M. Matsuura, J. Mater. Sci. 21, 2207 [1986].

## LABORATORY OPERATIONS

The Aerospace Corporation functions as an "architect-engineer" for national security projects, specializing in advanced military space systems. Providing research support, the corporation's Laboratory Operations conducts experimental and theoretical investigations that focus on the application of scientific and technical advances to such systems. Vital to the success of these investigations is the technical staff's wide-ranging expertise and its ability to stay current with new developments. This expertise is enhanced by a research program aimed at dealing with the many problems associated with rapidly evolving space systems. Contributing their capabilities to the research effort are these individual laboratories:

Aerophysics Laboratory: Launch vehicle and reentry fluid mechanics, heat transfer and flight dynamics; chemical and electric propulsion, propellant chemistry, chemical dynamics, environmental chemistry, trace detection; spacecraft structural mechanics, contamination, thermal and structural control; high temperature thermomechanics, gas kinetics and radiation; cw and pulsed chemical and excimer laser development including chemical kinetics, spectroscopy, optical resonators, beam control, atmospheric propagation, laser effects and countermeasures.

Chemistry and Physics Laboratory: Atmospheric chemical reactions, atmospheric optic, light scattering, state-specific chemical reactions and radiative signatures of missile plumes, sensor out-of-field-of-view rejection, applied laser spectroscopy, laser chemistry, laser optoelectronics, solar cell physics, battery electrochemistry, space vacuum and radiation effects on materials, lubrication and surface phenomena, thermionic emission, photo-sensitive materials and detectors, atomic frequency standards, and environmental chemistry.

Computer Science Laboratory: Program verification, program translation, performance-sensitive system design, distributed architectures for spaceborne computers, fault-tolerant computer systems, artificial intelligence, micro-electronics applications, communication protocols, and computer security.

Electronics Research Laboratory: Microelectronics, solid-state device physics, compound semiconductors, radiation hardening; electro-optics, quantum electronics, solid-state lasers, optical propagation and communications; microwave semiconductor devices, microwave/millimeter wave measurements, diagnostics and radiometry, microwave/millimeter wave thermionic devices; atomic time and frequency standards; antennas, rf systems, electromagnetic propagation phenomena, space communication systems.

Materials Sciences Laboratory: Development of new materials: metals, alloys, ceramics, polymers and their composites, and new forms of carbon; non-destructive evaluation, component failure analysis and reliability; fracture mechanics and stress corrosion; analysis and evaluation of materials at cryogenic and elevated temperatures as well as in space and enemy-induced environments.

Space Sciences Laboratory: Magnetospheric, auroral and cosmic ray physics, wave-particle interactions, magnetospheric plasma waves; atmospheric and ionospheric physics, density and composition of the upper atmosphere, remote sensing using atmospheric radiation; solar physics, infrared astronomy, infrared signature analysis; effects of solar activity, magnetic storms and nuclear explosions on the earth's atmosphere, ionosphere and magnetosphere; effects of electromagnetic and particulate radiations on space systems; space instrumentation.